Monthly Notices
of the
ROYAL ASTRONOMICAL SOCIETY

MNRAS **466,** 3133–3142 (2017)
Advance Access publication 2016 December 15

doi:10.1093/mnras/stw3265

Implications of an updated ultraviolet background for the ionization mechanisms of intervening Ne VIII absorbers

Tanvir Hussain,[1,2]★ Vikram Khaire,[3]★ Raghunathan Srianand,[1] Sowgat Muzahid[4] and Amit Pathak[2]

[1]*Inter-University Centre for Astronomy and Astrophysics, Post Bag 4, Ganeshkhind, Pune 411 007, India*
[2]*Department of Physics, Tezpur University, Tezpur 784 028, India*
[3]*National Centre for Radio Astrophysics, Tata Institute of Fundamental Research, Pune 411 007, India*
[4]*Leiden Observatory, University of Leiden, PO Box 9513, NL-2300 RA Leiden, the Netherlands*

Accepted 2016 December 13. Received 2016 December 9; in original form 2016 September 1

ABSTRACT

Ne VIII absorbers seen in QSO spectra are useful tracers of warm ionized gas, when collisional ionization is the dominant ionization process. While photoionization by the ultraviolet background (UVB) is a viable option, it tends to predict large line-of-sight thickness for the absorbing gas. Here, we study the implications of the recently updated UVB at low z to understand the ionization mechanisms of intervening Ne VIII absorbers. With the updated UVB, one typically needs higher density and metallicity to reproduce the observed ionic column densities under photoionization. Both reduce the inferred line-of-sight thicknesses of the absorbers. We find a critical density of $\geq 5 \times 10^{-5}$ cm^{-3} above which the observed N(Ne VIII)/N(O VI) can be reproduced by pure collisional processes. If the gas is of near solar metallicity (as measured for the low ions) then the cooling time-scales will be small ($<10^8$ yrs). Therefore, a continuous injection of heat is required in order to enhance the detectability of the collisionally ionized gas. Using photoionization models we find that in almost all Ne VIII systems the inferred low ion metallicity is near solar or supersolar. If we assume the Ne VIII phase to have similar metallicities then photoionization can reproduce the observed N(Ne VIII)/N(O VI) without the line-of-sight thickness being unreasonably large and avoids cooling issues related to the collisional ionization at these metallicities. However, the indication of broad Lyα absorption in a couple of systems, if true, suggests that the Ne VIII phase is distinct from the low ion phase having much lower metallicity.

Key words: intergalactic medium – quasars: absorption lines – diffuse radiation.

1 INTRODUCTION

The early measurements of abundances of deuterium along the line of sight to distant QSOs (Burles & Tytler 1998; O'Meara et al. 2006; Pettini et al. 2008) and cosmic microwave background (CMB) observations (Spergel et al. 2003; Komatsu et al. 2011) provided a good estimation of the baryonic content in the Universe. A recent census of baryons at $z \lesssim 0.4$, reported by Shull, Smith & Danforth (2012b), reveals that 28 ± 11 per cent of the baryons reside in photoionized intergalactic medium (IGM) traced by the Lyα forest (Rauch et al. 1997; Penton, Stocke & Shull 2004), 18 ± 4 per cent are observed in stars and cold interstellar medium in galaxies, circumgalactic medium (CGM) and X-ray emitting gas in clusters of galaxies and 25 ± 8 per cent are found in the warm-hot intergalactic medium (WHIM) traced by broad Lyα (BLAs) and O VI absorbers. The remaining 29 ± 13 per cent, the so-called 'missing baryons', are thought to reside in the hot phase of WHIM with gas densities in the range $n_{\rm H} \sim 10^{-6}$–10^{-5} cm^{-3}, temperatures in the range $T \simeq 10^5$–10^7 K (Persic & Salucci 1992; Davé et al. 2001) and baryonic overdensity $\Delta \sim$ 1–100 (Nevalainen et al. 2015). In comparison, H I Lyα forest absorption seen in QSO spectra at these low-z originate from baryonic overdensities of ∼1–30 covering N(H I) = 10^{12}–10^{14} cm^{-2} (see table 2 of Gaikwad et al. 2016a).

Since WHIM is hot and tenuous, it is best probed through X-ray absorption spectroscopy. An additional ∼15 per cent of the baryons could reside in the hot ($T > 10^6$ K) X-ray absorbing gas traced by the O VII λ21.602 (Nicastro et al. 2005a, b; Nicastro, Mathur & Elvis 2008; Buote et al. 2009; Fang et al. 2010; Zappacosta et al. 2010) and O VIII λ18.969 absorption lines (Fang et al. 2002; Fang, Canizares & Yao 2007). However, due to the lack of instruments capable of high-resolution and high-S/N X-ray spectroscopy (Yao et al. 2012; Nicastro et al. 2013; Ren, Fang & Buote 2014; Génova-Santos et al. 2015), one has to rely on detecting WHIM through

★ E-mail: tanvir@iucaa.in (TH); kvikram@ncra.tifr.res.in (VK)

far-ultraviolet (FUV, $900 < \lambda(\text{Å}) < 3000$) absorption lines in the spectra of QSOs. FUV spectrographs viz., Space Telescope Imaging Spectrograph (STIS), Cosmic Origins Spectrograph (COS) on board the *Hubble Space Telescope* (*HST*) and the *Far Ultraviolet Spectroscopy Explorer* (*FUSE*) have better resolution and S/N, which enable one to detect O VI λλ1031,1037 (e.g. Tripp, Savage & Jenkins 2000; Richter et al. 2004; Danforth & Shull 2005, 2008; Tripp et al. 2008) and Ne VIII λλ770,780 (e.g. Savage et al. 2005; Narayanan, Wakker & Savage 2009; Narayanan et al. 2011) absorption lines. Collisional ionization equilibrium (CIE) models of Gnat & Sternberg (2007) show that both O VI and Ne VIII can be good tracers of the low-temperature end of the WHIM having temperatures in the range $T \sim 10^{5.5}$–$10^{5.7}$ K.

To understand which ionizing mechanism (photoionization or collisional ionization or a combination of both) leads to the formation of such highly ionized species, it is necessary to have the ionizing ultraviolet background (UVB) radiation modelled accurately. The UVB spectrum decides (i) the derived metallicity of the gas, (ii) the density at which the observed N(Ne VIII)/N(O VI) can be produced and (iii) the critical density above which the gas will be in pure collisional equilibrium. All these are important to decide the mechanism that keeps the Ne VIII phase ionized.

The spectrum of UVB cannot be observed directly, however, can be modelled by a detailed radiative transfer of UV photons through the IGM (see Miralda-Escude & Ostriker 1990; Shapiro, Giroux & Babul 1994; Haardt & Madau 1996; Fardal, Giroux & Shull 1998; Shull et al. 1999). It involves using various observables as inputs such as QSO and galaxy luminosity functions (Schmidt 1967; Schechter 1976), spectral energy distribution (SED) of QSOs (Telfer et al. 2002), the fraction ($f_{\rm esc}$) of H I ionizing photons escaping from galaxies (Leitherer et al. 1995; Heckman et al. 2001) and the effective opacity of the IGM (Petitjean et al. 1993). The $f_{\rm esc}$ is one of the most uncertain observables and plays a significant role in determining the spectrum of UVB (see Khaire & Srianand 2013). At low-z, observations of a sample of galaxies provide a 3σ upper limit on $f_{\rm esc}$ to be less than 2 per cent (Cowie, Barger & Trouille 2009; Bridge et al. 2010; Siana et al. 2010; Rutkowski et al. 2016). The H I photoionization rate ($\Gamma_{\rm H\,I}$) measurements obtained using various methods (see Sunyaev 1969; Bajtlik, Duncan & Ostriker 1988; Dove & Shull 1994; Vogel et al. 1995; Srianand & Khare 1996; Savaglio et al. 1997) can be used to constrain the values of $f_{\rm esc}$ (see for e.g. Inoue, Iwata & Deharveng 2006; Khaire et al. 2016) while modelling the UVB.

The recent studies of H I column density distribution of low-z Lyα forest, using *HST*/COS data (Danforth et al. 2016), show that the $\Gamma_{\rm H\,I}$ at low redshifts (i.e. $z < 1.0$) is a factor of 2–5 times higher (Kollmeier et al. 2014; Shull et al. 2015; Wakker et al. 2015; Gaikwad et al. 2016b) than what is predicted by the UVB model of Haardt & Madau (2012, hereafter, HM12). This discrepancy, pointed out as a crisis in the photon production (Kollmeier et al. 2014), is resolved by Khaire & Srianand (2015a, hereafter, KS15) using the updated QSO luminosity function (i.e. Croom et al. 2009; Palanque-Delabrouille et al. 2013) and star formation history of low-z galaxies (Khaire & Srianand 2015b). It is found that, $\Gamma_{\rm H\,I}$ obtained using only the updated QSO emissivity (i.e. with no galaxy contribution to the UVB or $f_{\rm esc} = 0$ per cent), is a factor of 2 higher than that of HM12 UVB at $z < 0.5$. This is also consistent with the $\Gamma_{\rm H\,I}$ measurements by Shull et al. (2015). With a constant $f_{\rm esc}$ of 4 per cent, the KS15 UVB provides five times higher $\Gamma_{\rm H\,I}$ than HM12 at $z < 0.5$ consistent with the Kollmeier et al. (2014) measurements. However, the latest $\Gamma_{\rm H\,I}$ measurements by Gaikwad et al. (2016a,b), Gurvich, Burkhart & Bird (2016) and Viel et al. (2016) favour results of Shull et al. (2015). Gaikwad et al. (2016a) measured $\Gamma_{\rm H\,I}$ in four redshift bins at $z \lesssim 0.45$ using two different statistics and also provided a good accounting of associated statistical and systematic errors. Their measurements are well reproduced by KS15 UVB with $f_{\rm esc} = 0$ per cent and provide a 3σ upper limit of 0.8 per cent for the $f_{\rm esc}$ at $z < 2$. Therefore, in analysis presented in this work we use KS15 UVB with $f_{\rm esc} = 0$ per cent.

Using the previously published extragalactic UVBs, i.e. Haardt & Madau (1996, hereafter, HM96), Haardt & Madau (2001, hereafter, HM01), HM05[1] and HM12 as the incident radiation, it has been found that the observed properties of O VI in the low-z IGM can be understood by both photoionization (Thom & Chen 2008; Tripp et al. 2008; Howk et al. 2009; Muzahid et al. 2012, 2015) as well as collisional ionization models (Danforth & Shull 2008). On the other hand, for the Ne VIII absorbers detected so far (summarized in Table 1), photoionization was not favoured (but see Hussain et al. 2015, for an exception) based on extremely large line-of-sight thickness (i.e. >1 Mpc) inferred from the photoionization models. Therefore, the previous studies of Ne VIII systems (Savage et al. 2005; Narayanan et al. 2009, 2011; Narayanan, Savage & Wakker 2012; Meiring et al. 2013) favour these absorbers originating from a gas collisionally ionized at $T \approx 10^{5.4}$–$10^{5.7}$ K and thus could harbour a vast reservoir of baryons evident from their high inferred total hydrogen column densities ($N_{\rm H} \sim 10^{19}$–10^{20} cm^{-2}). Presence of BLA absorption associated with the Ne VIII components will favour this picture (see for example, Savage et al. 2011).

In this work, using the recently updated UVB, we revisit the ionization scenarios for the Ne VIII absorbers at low-z. This paper is organized as follows: In Section 2, we describe the updated UVB. Discussion on the various ionization models for Ne VIII systems are explored in Section 3. Reanalysis of the Ne VIII absorbers with the updated UVB and the results are given in Section 4. In Section 5, we summarize our conclusions. Throughout this paper, we adopt an $H_0 = 70\,{\rm km\,s^{-1}\ Mpc^{-1}}$, $\Omega_{\rm m} = 0.3$ and $\Omega_\Lambda = 0.7$ flat cosmology (Komatsu et al. 2011). The solar relative abundances for the heavy elements are taken from Grevesse et al. (2010).

2 UPDATED UVB AND NE VIII SYSTEMS

In this work, we study the implications of using the KS15 UVB in the photoionization models on the inferred densities, metal abundances and line-of-sight thickness of the known Ne VIII absorbers. KS15 UVB uses an updated QSO emissivity and star formation rate density (Khaire & Srianand 2015b). To analyse the Ne VIII systems, we use KS15 UVB generated for $f_{\rm esc} = 0$ per cent consistent with $\Gamma_{\rm H\,I}$ measurements of Shull et al. (2015) and Gaikwad et al. (2016a).

In Fig. 1, we plot the KS15 UVB spectrum (energy E vs specific intensity J_ν) for $f_{\rm esc} = 0$ per cent at $z = 0.2$. For comparison, we also show the HM96, HM05 and HM12 UVBs at that redshift. The dotted vertical lines mark the ionization energies of different ions of carbon, nitrogen, oxygen and neon. Clearly from this figure, we see that the ionization energies of highly ionized species (such as O V, O VI, O VII, Ne VII, Ne VIII and Ne IX) fall beyond the He II ionization energy, i.e. $E > 4$ Ryd. At these energies, since galaxies do not show any emission, the UVB is solely contributed by QSOs irrespective of the $f_{\rm esc}$ value. Additionally at these energies, the intensity of the UVB depends on the average SED that is used to estimate the QSO emissivity. The QSO SEDs over large wavelength

[1] HM05 is the unpublished extragalactic UVB described in HM01 and is included for use in CLOUDY (see Ferland et al. 2013, for detailed description).

Table 1. Properties of intervening Ne VIII absorbers from the literature.

QSO	z_{abs}	log[N(O VI)][a] (cm^{-2})	log[N(Ne VIII)][a] (cm^{-2})	log [N_H][b] (cm^{-2})	log[N(H I)][c] (cm^{-2})	[X/H][d]	Line-of-sight thickness[e] (Mpc)	UVB used for PI model	Ref.
HE 0226−4110	0.20701	14.38 ± 0.01	13.89 ± 0.11	20.06	13.87	−0.5	∼11	HM96	[AI]
3C 263	0.32566	13.98 ± 0.05	13.99 ± 0.11	19.50	13.20	−0.38	∼5.6	HM96	[AII]
PKS 0405−123	0.49509	14.39 ± 0.01[f]	13.96 ± 0.06[f]	19.70[g]	$\lesssim$13.50	−1.0	∼2.5	HM01	[AIII]
PG 1148+549	0.68381	14.41 ± 0.02	13.95 ± 0.04	19.80	13.60	−0.5	$\gtrsim$1	HM96 + HM01	[AIV]
PG 1148+549	0.70152	14.28 ± 0.03	13.82 ± 0.06	19.00	<12.80	>0.2	$\gtrsim$1	HM96 + HM01	[AV]
PG 1148+549	0.72478	13.86 ± 0.07	13.81 ± 0.06	18.90	<12.60	>0.0	$\gtrsim$1	HM96 + HM01	[AVI]
PG 1407+265	0.59961	13.67 ± 0.09[h]	13.65 ± 0.19[h]	19.65	<13.40	0.0	∼0.186[i]	HM05	[AVII]

Notes. [a]Voigt profile fitted column density measured for the component at $v_{rel} = 0$ km s^{-1}, co-aligned in velocity with the low ions detected in the respective spectra.
[b]The total hydrogen column density N_H as inferred from the CIE models.
[c]The neutral hydrogen column density N(H I) associated with broad Ne VIII-gas component consistent with the CIE models.
[d][X/H] ($\equiv$ log [X/H]$_{obs}$ − log [X/H]$_\odot$) is the logarithmic metallicity with respect to solar abundances for the low ionized species as calculated from photoionization models.
[e]Line-of-sight thickness as measured from photoionization models for the high ions (Ne VIII and O VI).
[f]Measured using the apparent optical depth (AOD) method (Savage & Sembach 1991).
[g]Computed assuming a hybrid (photoionization + collision) ionization model.
[h]The column density of Ne VIII and O VI is for the component at $v_{rel} = -150$ km s^{-1}.
[i]Line-of-sight thickness of ∼175 kpc was reported using HM12 UVB and solar metallicity.
References: [AI] Savage et al. (2005, 2011), [AII] Narayanan et al. (2009, 2012), [AIII] Narayanan et al. (2011), [AIV, AV, AVI] Meiring et al. (2013), [AVII] Hussain et al. (2015).

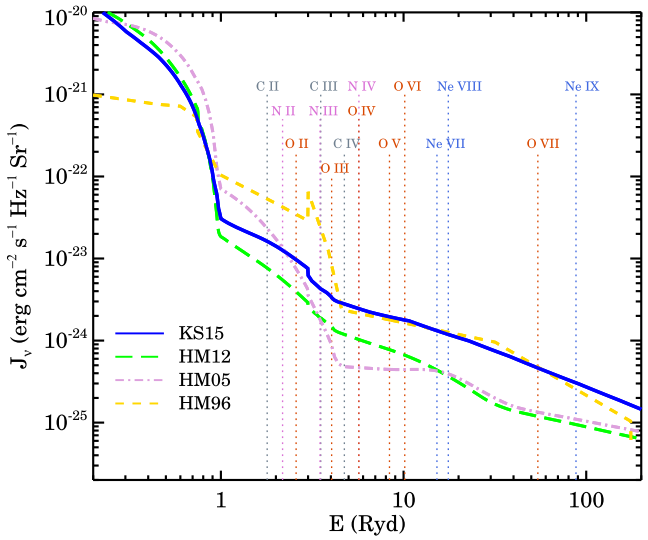

Figure 1. The KS15 UVB spectrum at redshift $z = 0.2$ is shown as the blue continuous curve. For comparison, we also show the HM96, HM05 and HM12 UVBs at the same z in yellow, purple and green dashed curves, respectively. The vertical dotted lines (in different colours) mark the ionization energies of different ions of carbon, nitrogen, oxygen and neon as indicated.

range can be approximated by a power law of the form $L_\nu \propto \nu^\alpha$ (Francis et al. 1991; Vanden Berk et al. 2001; Scott et al. 2004; Shull, Stevans & Danforth 2012a). Following Stevans et al. (2014), KS15 UVB uses $\alpha = -1.41$ at $\lambda < 1000$ Å while HM12 uses $\alpha = -1.57$ (Telfer et al. 2002). Note that, the power law has been observed only up to 2 Ryd (i.e. for $\lambda > 475$ Å, Stevans et al. 2014), which is extrapolated to higher energies in UVB models. At $E > 4$ Ryd, the KS15 UVB has a factor of ∼3 higher intensity compared to HM12 due to the use of updated QSO emissivity and SED. The low ionized species (such as O II, O III, N II, N III, C III) have ionization energies $E = 1$−4 Ryd. At these energies, the UVB is contributed by radiation from QSOs as well as galaxies. The contribution of galaxies depends on the assumed value of f_{esc}. Since we are using the KS15 UVB with $f_{esc} = 0$ per cent, only QSOs contribute to UVB. Here, the KS15 UVB has a factor of 2 higher intensity due to the updated QSO emissivity.

In Table 1, we list the seven Ne VIII systems[2] detected along the line of sight of five QSOs. The range of the absorption redshift covered by these systems is $z_{abs} = 0.2$–0.7. In all these cases, Ne VIII absorption is co-aligned in velocity space with the O VI absorption. Therefore, as is the case in most of the previous studies of Ne VIII absorbers, we will assume O VI and Ne VIII to be co-spatial. The column densities of Ne VIII and O VI are well measured in these systems. Using previous UVBs, i.e. HM96, HM01 and HM05, photoionization models of most of the systems suggested a large line-of-sight thickness of >1 Mpc (as provided in Table 1). At such large thickness, the width of the Ne VIII absorption due to the expansion of the universe will be much larger than the observed width, $b_{Ne\,VIII}$, which is in the range of 23–70 km s^{-1}, thereby ruling out a photoionized origin of Ne VIII. However, there is only one system where photoionization could explain the observed Ne VIII with the line-of-sight thickness measured being ∼186 kpc (detected at $z_{abs} = 0.59961$ towards PG 1407+265, Hussain et al. 2015). Therefore, apart from this system, all the other Ne VIII systems are suggested to be originating from a collisionally ionized gas at temperatures log[T(K)] = 5.4−5.7 with inferred line-of-sight thickness (l) $\lesssim$ 100 kpc. At these high temperatures, one expects the ionization fraction of H I, $f_{HI} \sim 6 \times 10^{-7}$ in the collisional ionization models of Gnat & Sternberg (2007). For N_H in the range 10^{19}–10^{20} cm^{-2}, as suggested by the models, the expected N(H I) is $6 \times (10^{12}$–$10^{13})$ cm^{-2} and the b-parameter

[2] We do not list the Ne VIII systems detected at $z_{abs} = 0.927$ towards PG 1206+549 by Tripp et al. (2011), as the authors do not provide the column density measurement of O VI, which is important in our analysis. Also, we do not list the Ne VIII absorption detected towards QSO J1154+4635 by Bordoloi, Heckman & Norman (2016) as no information about the absorption redshift or of the low ionized species is provided, which are also important in our analysis.

of the absorption is in the range 66–93 km s^{-1}. This will produce a BLA associated with the Ne VIII absorption. Based on the presence of excess absorption in the wings of the Lyα absorption, on top of the absorption profile predicted from the higher Lyman series lines, N(H I) associated with the Ne VIII is measured in the case of two systems: $z_{\rm abs} = 0.20701$ towards HE 0226−4110 (Savage et al. 2005, 2011) and $z_{\rm abs} = 0.32566$ towards 3C 263 (Narayanan et al. 2009, 2012). For the remaining five absorbers, Lyα absorption is not covered in the COS spectrum. For, $z_{\rm abs} = 0.70152$ and 0.72478 systems towards PG1148+549 (Meiring et al. 2013) and one of the Ne VIII components for the $z_{\rm abs} = 0.59961$ towards PG1407+265 (Hussain et al. 2015), no H I absorption is detected through Lyβ or higher Lyman series lines. The lack of direct detection of BLAs in these cases suggests that if the gas is collisionally ionized than the metallicity has to be higher.

Here, we reanalyse all these Ne VIII systems in the framework of photoionization by the KS15 UVB using CLOUDY (v13.03; Ferland et al. 2013). We assume the absorbing gas to be plane-parallel slabs of constant density having relative abundances as observed in the solar photosphere (Grevesse et al. 2010). To understand the ionization mechanisms of these absorbers, we first explore the total hydrogen density $n_{\rm H}$ and temperature T range of the gas giving rise to the observed N(Ne VIII)/N(O VI). Constraints on $n_{\rm H}$ and metallicity Z[3] will give the line-of-sight thickness l of the Ne VIII bearing gas cloud that is determined using the following equation:

$$l = \frac{N_{\rm Ne\,VIII}}{n_{\rm H} f_{\rm Ne\,VIII}} \frac{1}{Z} \left(\frac{\rm Ne}{\rm H}\right)^{-1}_{\odot}$$

$$\simeq 200\,{\rm kpc} \left(\frac{N_{\rm Ne\,VIII}}{10^{14}}\right) \left(\frac{n_{\rm H}}{10^{-5}}\right)^{-1} \left(\frac{f_{\rm Ne\,VIII}}{0.18}\right)^{-1} \left(\frac{1}{Z}\right) \left(\frac{\rm Ne}{\rm H}\right)^{-1}_{\odot}. \quad (1)$$

Here, $f_{\rm Ne\,VIII} \equiv n_{\rm Ne\,VIII}/n_{\rm Ne}$ is the ionization fraction of Ne VIII (as computed by CLOUDY) and $(\frac{\rm Ne}{\rm H})_{\odot} = -4.07$ is the solar relative abundance of neon. Therefore, to determine l, we need to obtain the metallicity of the gas associated with the Ne VIII phase. In the absence of N(H I) measurements from the Ne VIII phase, one assumes the gas phase metallicity of the Ne VIII phase to be similar to the low ionization phase. As we pointed out before, to estimate the metallicity of low ions, the assumed spectrum of UVB is crucial.

3 IONIZATION MODELS FOR NE VIII SYSTEMS

As a demonstration of our approach, we run CLOUDY models for $z = 0.2$. Initially, to see the effect of UVB on the derived $n_{\rm H}$, we compute the ratio of N(Ne VIII)/N(O VI) as a function of $n_{\rm H}$ under the photoionization equilibrium for KS15 and HM12 UVB. The results are shown in Fig. 2. It is clear from this figure that for any observed value of N(Ne VIII)/N(O VI), the $n_{\rm H}$ determined using KS15 UVB is a factor of ∼3 higher than what we find using HM12 UVB. Therefore, for a given metallicity and N(H), l calculated for the KS15 UVB will be three times smaller[4] as compared to that derived using the HM12 UVB. There is a constant shift along the density axis between the two models as the spectral shape of the two UVBs are similar in the energy range of interest (see Fig. 2). As mentioned earlier, these high ions are affected by the UVB photons with $E > 4$ Ryd where the contribution to UVB depends both on QSO emissivities as well as on the average SED of the QSOs. Therefore, we also run CLOUDY models with KS15 UVB generated for $\alpha = -1.26$ to -1.56 consistent within 1σ range in α (=-1.41 ± 0.15) measured by Stevans et al. (2014). The resultant ratio of N(Ne VIII)/N(O VI) is shown in as grey-shaded region in Fig. 2. Taking into account this uncertainty in SED, the measured $n_{\rm H}$ (and hence l) is a factor of ∼2–5 higher (smaller) as compared to the one derived using the HM12 UVB. Note that, in all these models, the temperature ($T \sim 3$–8×10^4 K) of the gas is self-consistently calculated by CLOUDY, which mainly arises due to photoheating by the UVB. However, in the cosmological hydrodynamical simulations the gas temperature at a given $n_{\rm H}$ can also be decided by other heating and cooling processes. In order to account for this, we need to consider models over the temperature density plane from which Ne VIII systems can originate (see for example, Tepper-García, Richter & Schaye 2013).

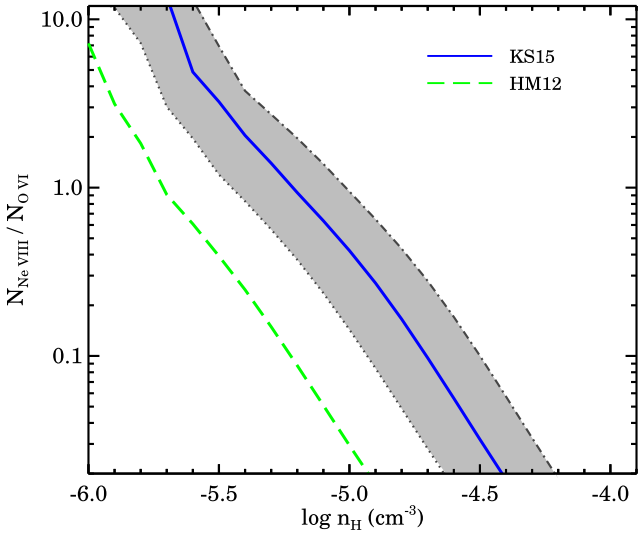

Figure 2. Results of photoionization model for Ne VIII and O VI for an absorber at $z = 0.2$ using KS15 and HM12 UVB. Blue line represents the model predicted ratio for KS15 UVB while the dashed green line is for HM12 UVB. The grey shaded region shows the results of the photoionization model using KS15 UVBs generated with different QSO SED by changing $\alpha = -1.26$ (in dot–dashed curve) to -1.56 (in dotted curve) covering 1σ range in α as measured by Stevans et al. (2014). For a given (Ne VIII/O VI) ratio, $n_{\rm H}$ from KS15 model is a factor of ∼2–5 higher than that of HM12. This is due to the updated QSO emissivity used in KS15 UVB.

We ran several CLOUDY models in the presence of different UVBs at $z = 0.2$ on a grid of constant temperatures and $n_{\rm H}$ to reproduce the observed range in the column density ratios of Ne VIII to O VI (i.e. 0.33–1.02, see Table 1) and the results are shown in Fig. 3. We refer to these models as 'hybrid models'. In the left-hand panel of Fig. 3, the hatched region with vertical blue lines and horizontal green lines show the allowed range in the $n_{\rm H}$–T plane from where N(Ne VIII)/N(O VI) constraints can be obtained in the case of KS15 and HM12 UVBs, respectively. Irrespective of the UVB model, the required $n_{\rm H}$ increases slowly with increasing gas temperature up to a certain temperature and then it rapidly diverges after a critical density (i.e. $n_{\rm H} \sim 2 \times 10^{-5}$ cm^{-3} for HM12 and $\sim 5 \times 10^{-5}$ cm^{-3} for KS15). The region of $n_{\rm H}$–T plane where $n_{\rm H}$ increases slowly

[3] Z is the linear metal abundance of the absorber with respect to solar photospheric abundances.

[4] Note that, the KS15 UVB uses the cloud distribution as provided in HM12. We also model these Ne VIII systems using the UVB generated with Inoue et al. (2014) cloud distribution and find the photoionization model results to be similar to KS15 UVB.

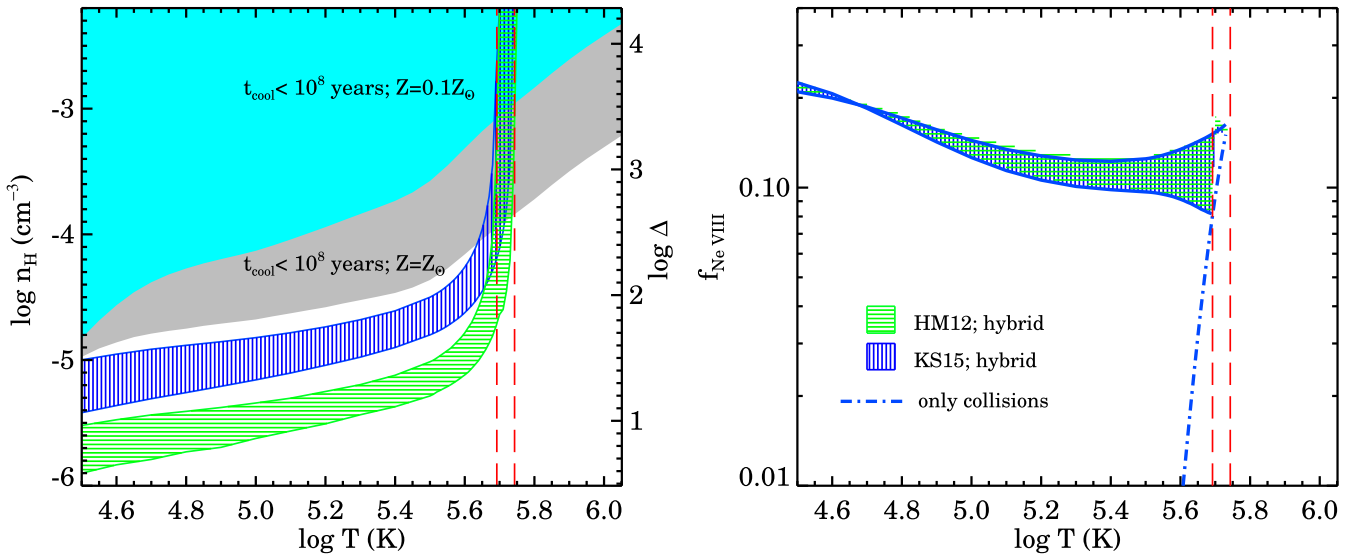

Figure 3. Left-hand panel: the $n_{\rm H}$–T plane showing the origin of observed Ne VIII systems at $z = 0.2$ obtained to satisfy the observed ratio of Ne VIII to O VI column densities. The hatched region with vertical blue lines and horizontal green lines show the $n_{\rm H}$–T plane from where Ne VIII systems can arise in the presence of KS15 and HM12 UVBs, respectively. The grey and cyan shaded regions show $n_{\rm H}$–T plane where the cooling time scales to reach $T = 10^4$ K is less than 10^8 yrs for gas with $Z = Z_{\odot}$ and $Z = 0.1Z_{\odot}$, respectively. Red dash line shows the region dominated by collisions. We also show the overdensities (Δ) measured corresponding to each $n_{\rm H}$. Right-hand panel: the ionization fraction of Ne VIII, $f_{\rm Ne\,VIII}$, with temperature from hybrid models of left-hand panel for KS15 and HM12 UVBs at $z = 0.2$. The $n_{\rm H}$ at each T is taken from the left-hand panel for the respective UVB models. The dot–dashed line shows $f_{\rm Ne\,VIII}$ only from collisions. Red dash lines are same as in the left-hand panel.

is dominated by photoionization. This slow increase is mainly due to the temperature dependence of the recombination coefficients of several ions. The small region in the $n_{\rm H}$–T plane where $n_{\rm H}$ increases rapidly is dominated by collisions. To show the relative contribution of collisions to the Ne VIII production, in the right-hand panel of Fig. 3, we show the ionization fraction of Ne VIII, $f_{\rm Ne\,VIII}$, as a function of temperature. At each temperature, the $n_{\rm H}$ is taken from $n_{\rm H}$–T plane for the respective UVB model as shown in the left-hand panel of Fig. 3. The $f_{\rm Ne\,VIII}$ form collision peaks sharply at a very small temperature range. It is comparable to the $f_{\rm Ne\,VIII}$ obtained in the hybrid model with $5.68 < \log T({\rm K}) < 5.74$ as shown in the left-hand panel of Fig. 3.

Given the high densities inferred for the gas to be in CIE in the presence of UVB (i.e. the baryonic overdensity $\Delta > 100$, see the left-hand panel of Fig. 3), the gas at the above mentioned range in temperature can cool very efficiently. We estimate the cooling time, $t_{\rm cool}$, the time required by the gas in $n_{\rm H}$–T plane to reach $T = 10^4$ K, using the cooling curves of Schure et al. (2009). The grey and cyan shaded regions in the left-hand panel of Fig. 3 show the region of $n_{\rm H}$–T plane that can cool in $t_{\rm cool} < 10^8$ yr, for a gas with metallicities $Z_{\odot}$ and $0.1Z_{\odot}$, respectively. It suggests that most of the collisionally ionized Ne VIII systems can cool very fast to the temperatures where Ne VIII can originate from photoionization. Now the cooling can be isochoric (constant density) or isobaric (constant pressure): i.e. increasing density with decreasing temperature. We consider an isochoric cooling gas [i.e. a gas with a constant $n_{\rm H} = 10^{-4}$ cm^{-3}, which is the critical density above which the N(Ne VIII)/N(O VI) ratio can be produced by collisional ionization] in the presence of UVB in Fig. 4. The model-predicted N(Ne VIII)/N(O VI) ratio at low temperatures is at least an order of magnitude lower than the observed ratio. The situation will be worse in the case of isobaric where one expects the density to be higher at low T. Therefore, in order for the collisionally ionized gas to reproduce the observed N(Ne VIII) and N(Ne VIII)/N(O VI) ratio, one needs to avoid the rapid

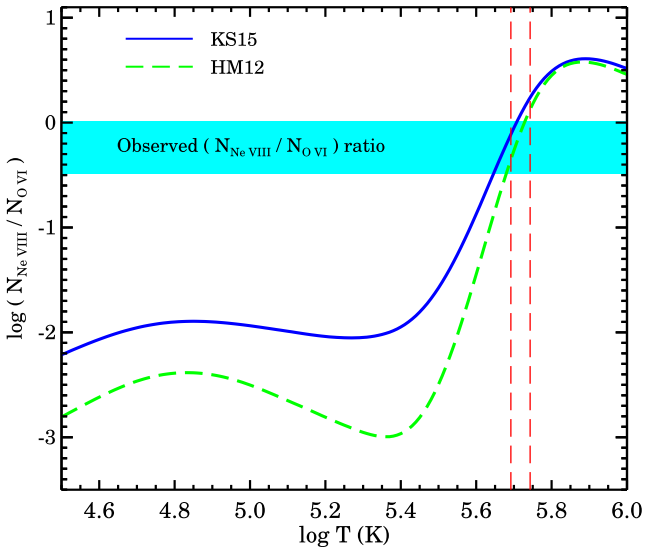

Figure 4. A 'hybrid' photoionization model computed for $z = 0.2$ assuming the gas to be isochoric i.e. having a constant density. We choose a constant density $n_{\rm H} = 10^{-4}$ cm^{-3} as it is the critical density above which the (Ne VIII/O VI) ratio can be produced with collisional ionization. The green and blue curves represent the model solutions for the HM12 and KS15 UVBs, respectively. The shaded region represents the observed column density ratio of Ne VIII/O VI while the red dotted lines show the region dominated by collisions. At low temperatures, the model predicted N(Ne VIII)/N(O VI) is at least an order of magnitude lower than the observed ratio.

cooling. This rapid cooling issue can be avoided if we have (i) the gas metallicity to be low (i.e. $Z < 0.1Z_{\odot}$) or (ii) the cloudlets containing this gas are being continuously pumped by mechanical energy from nearby sources at a rate that can compensate the inferred cooling rate.

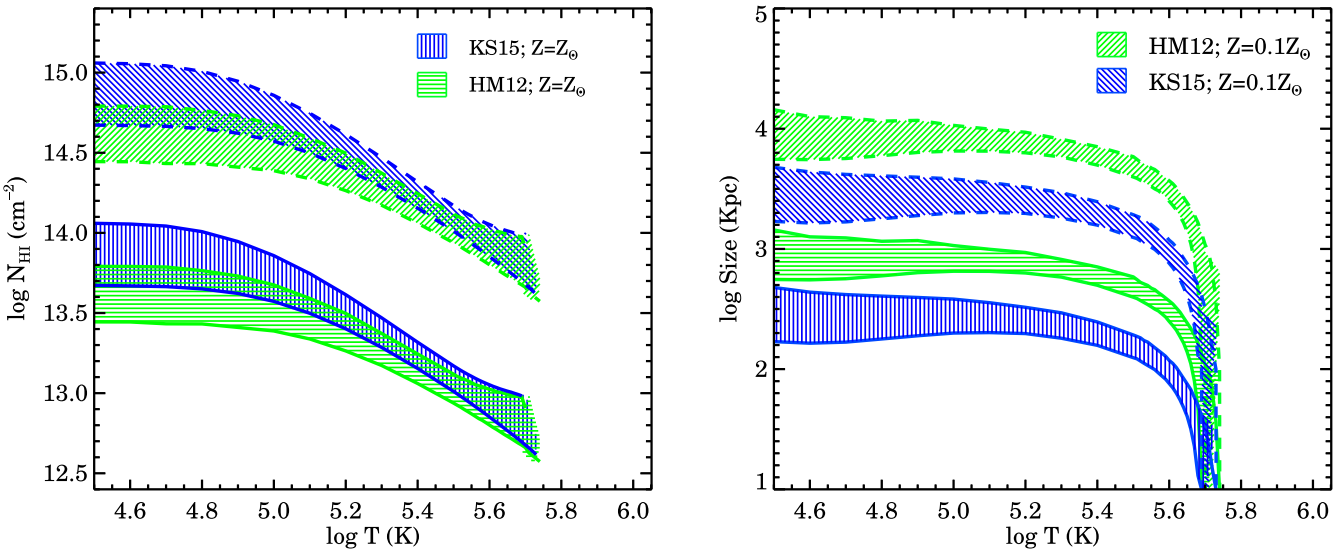

Figure 5. Left-hand panel: the N(H I) associated with Ne VIII system at $z = 0.2$ at different constant temperatures. The blue and green hatched regions are the N(H I) in the presence of KS15 and HM12 UVBs, respectively. Here, we assumed N(Ne VIII) $= 10^{14}$ cm^{-2} consistent with the observations. Results are shown for the gas with $Z = Z_{\odot}$ and $Z = 0.1Z_{\odot}$, respectively. Right-hand panel: the line-of-sight thickness of Ne VIII systems with temperature at $z = 0.2$ in the presence of KS15 and HM12 UVBs. For each model, the $n_{\rm H}$ is taken from the $n_{\rm H}$–T plane of Fig. 3 (left-hand panel).

In the left-hand panel of Fig. 3, we also show the overdensities (Δ) corresponding to each $n_{\rm H}$ [from $n_{\rm H} = 1.9 \times 10^{-7}(cm^{-3})(1+z)^3\Delta$]. Large overdensities ($\Delta > 300$ for KS15 UVB; $\Delta > 80$ for HM12 UVB) are required to maintain the CIE within $5.68 < \log T$(K) < 5.74 (where collisions dominate). Such overdensities reveal that the absorbers should originate in a dense galactic environment or from hot haloes. This is consistent with the detection of a disc galaxy in the vicinity of the Ne VIII absorber towards HE 0226−4110 (Mulchaey & Chen 2009) with luminosity $L = 0.25\ L_{\star}$, at an impact parameter $\rho = 109$ kpc. Here, $L_{\star}$ is the characteristic galaxy luminosity. Other than the above absorber, three absorbers at $z_{\rm abs} = 0.49509$ towards PKS 0405−123, 0.72478 towards PG 1148+549 and 0.59961 towards PG 1407+265 are also found to be associated with L $= 0.08\ L_{\star}$, L $= L_{\star}$ and a sub-$L_{\star}$ galaxy at an impact parameter of 110 (Chen & Mulchaey 2009), 217 (Meiring et al. 2013) and 89 kpc (Werk, private communication), respectively, in their vicinities. But there is no direct detection of galaxies, although the measured metallicities are solar, for the absorber at $z_{\rm abs} = 0.32566$ towards 3C 263 (Narayanan et al. 2009, 2012).

We also calculate the N(H I) associated with the Ne VIII phase in these models. For the illustrative purpose, we take N(Ne VIII) $= 10^{14}$ cm^{-2}, consistent with the observations (see Table 1). The results are shown in the left-hand panel of Fig. 5 for a gas with the solar metallicities $Z_{\odot}$ and $0.1Z_{\odot}$. To get the observed N(H I) [i.e. $\log N$(H I) ~ 14] from the photoionized gas, the metallicity should be of the order of $Z_{\odot}$ and more. However, the collisionally ionized gas ($T > 10^{5.5}$ K) can have low metallicities ($0.1Z_{\odot} < Z < Z_{\odot}$). We have also calculated the line-of-sight thickness for these systems, as shown in the right-hand panel of Fig. 5. For the gas in photoionization equilibrium with the KS15 UVB model, the gas with metallicity $Z \geq Z_{\odot}$ can come from clouds with thickness $l \leq 400$ kpc. The thickness of the low metallicity clouds originating due to photoionization is too large to be physical. These systems are better explained with collisional ionizations since the gas with temperatures where collisions dominate, can come from very small clouds (as can be seen in the right-hand panel of Fig. 5). However, it is interesting to investigate the environment of such systems to study the mechanism keeping them at these temperatures. Moreover, to understand the ionization scenarios of Ne VIII absorbers, it is important to measure the metallicity and N(H I) of the gas.

4 REANALYSIS OF THE NE VIII ABSORBERS

Here we reanalyse the Ne VIII absorbers identified in Table 1 in the framework of photoionization using the KS15 UVB. For a few systems, Ne VIII absorption is seen in multiple components. For the sake of simplicity, in this work, we model the Ne VIII component at $v_{\rm rel} = 0$ km s^{-1}, unless otherwise specified. Owing to the non-detection of N(H I) associated with the Ne VIII phase, we assume the gas phase metallicity of this Ne VIII phase to be similar to what we derive from the low ionization phase. We use the column density ratios of O III/O IV, O IV/O III and/or N II/N III to constrain the low ionization gas phase density and hence measure the metallicity of this phase. We use this derived metallicity, assuming it to be similar to the metallicity of the high ionization phase, as an input in our photoionization model for Ne VIII phase. The density of the Ne VIII phase is constrained using the column density ratio of Ne VIII/O VI. Below we briefly discuss photoionization model of each of the Ne VIII systems.

4.1 HE 0226−4110 (Savage et al. 2005, 2011)

An Ne VIII absorber is detected along the line of sight of QSO HE 0226−4110 at $z_{\rm abs} = 0.20701$. Along with Ne VIII, a BLA is also detected having $\log[N$(H I)(cm^{-2})$] = 13.87 \pm 0.08$ and $b = 72^{+13}_{-6}$ km s^{-1}. For this absorber, using HM96 UVB, the authors ruled out a possible origin of Ne VIII under photoionization equilibrium. Assuming the low ion gas phase metallicity (i.e. [X/H] $= -0.5$) to be similar to the Ne VIII phase, their photoionization model solutions for Ne VIII are: $n_{\rm H} = 4.5 \times 10^{-7}$ cm^{-3} and line-of-sight thickness $l \sim 11$ Mpc.

Here, using the column density ratio N(O III)/N(O IV), we constrain the low ionization gas phase density and hence determine

Table 2. Reanalysis of Ne VIII absorbers under photoionization equilibrium using the KS15 UVB.

QSO	z_{abs}	Ion ratios used to constrain low ion gas density n_H	[X/H][a]	log $[n_H]^b$ (cm^{-3})	log$[N(H\,I)]^c$ (cm^{-2})	log $[N_H]$ (cm^{-2})	l^d (kpc)
HE 0226−4110	0.20701	O III/O IV	0.12	−4.90	13.90	18.56	94
3C 263	0.32566	O III/O IV	0.00	−5.10	13.59	18.86	299
PKS 0405−123	0.49509	O III/O IV	0.46	−4.50	13.69	18.14	22
PG 1148+549	0.68381	O IV/O III	0.32	−4.40	13.58	18.40	20
PG 1148+549	0.70152	O IV/O III	>0.95	−4.40	<12.86	<17.64	4
PG 1148+549	0.72478	O IV/O III	>0.79	−4.70	<12.54	<17.88	12
PG 1407+265	0.59961	N II/N III	>0.27[e]	−4.80	<12.90	<18.27	38

Notes. [a]Logarithmic metallicity with respect to solar photospheric abundances. The metallicities listed in the table for the high ions are measured from the low ion photoionization model, assuming them to be similar to the high ionization phase. The lower limits in metallicities are because of the non-detection of higher H I Lyman series absorption lines associated with the Ne VIII absorber.
[b]Total hydrogen density, n_H, associated with the photoionized Ne VIII gas phase as measured from the photoionization model.
[c]The neutral hydrogen column density associated with the photoionized Ne VIII gas phase.
[d]The line-of-sight thickness for each of the photoionized Ne VIII absorber is measured using equation (1).
[e]The metallicity measured for this absorber is based on oxygen (O II).

the metallicity of this phase to be [X/H] = 0.12. We use this measured metallicity in photoionization models for Ne VIII phase and the model solutions are listed in Table 2. With the updated UVB, we find the n_H to be ∼2 orders of magnitude more than what was derived earlier (using HM96 UVB). As a result, we obtain ∼2 orders of magnitude less line-of-sight thickness (l = 94 kpc) using KS15 UVB. Thus, owing to the small line-of-sight thickness measured, this Ne VIII absorber can have a photoionized origin.

However, if we assume, that H I column density associated with the Ne VIII to be a BLA as suggested by Savage et al. (2011), then from CIE models of Gnat & Sternberg (2007), the metallicity of the Ne VIII phase turns out to be [X/H] = −0.94 (is within errors of what have been reported by Savage et al. 2011). This metallicity is a factor of ∼12 less compared to that derived from photoionization model of low ions. From the discussions presented in Section 3, it is clear that the low metallicity gas has larger cooling time-scales and sustain the Ne VIII phase at a detectable level for a longer period of time. In summary, photoionization is a viable option for this system if the Ne VIII phase has the same metallicity as the low ion phase. However, if the BLA identified by Savage et al. (2011) is correct, then Ne VIII can be consistently produced by collisions with the absorbing gas having lower metallicity than that of the gas producing low ion absorption.

4.2 3C 263 (Narayanan et al. 2009, 2012)

Along with Ne VIII absorption at z_{abs} = 0.32566 towards the line of sight of QSO 3C 263, a BLA is also marginally detected with log$[N(H\,I)$(cm^{-2})] ∼ 13.20 and b = 93 km s^{-1}. For this absorber, from low ion photoionization model using HM96 UVB, the metallicity reported by Narayanan et al. (2009) is [X/H] = −0.38. Assuming this metallicity to be similar to the Ne VIII phase, the photoionization model solutions for the Ne VIII phase are: $n_H \sim 5.0 \times 10^{-6}$ cm^{-3}, $N_H \sim 10^{20}$ cm^{-2} and line-of-sight thickness ∼5.6 Mpc. Owing to the large thickness measured, the authors ruled out a photoionized origin for Ne VIII.

Here, like above, by using the column density ratio of N(O III)/N(O IV) as a constraint on low ionization gas density, we obtain the metallicity of the low ionization phase to be solar (i.e. [X/H] = 0.00). We use this measured metallicity in photoionization models for Ne VIII phase and the results are shown in Table 2. We find the n_H measured is a factor of ∼2 more than what was derived using HM96 UVB. As compared to HM96, we obtain much smaller line-of-sight thickness (l = 299 kpc) ensuring the Ne VIII absorber can have a photoionized origin.

If the BLA is associated with the warm Ne VIII phase, then under the collisional ionization models of Gnat & Sternberg (2007), we measure the metallicity to be [X/H] = −0.53. Like the above system, this absorber too can be produced via collisions provided we have gas metallicity of the high ion phase to be less than that of the low ion phase by a factor of ∼3.

4.3 PKS 0405−123 (Narayanan et al. 2011)

An Ne VIII absorber is detected at z_{abs} = 0.495 096 towards QSO PKS 0405−123. Using the HM01 UVB and solar metallicity in their photoionization models,[5] the authors reported that photoionization is not responsible for the production of Ne VIII in this absorber. Their photoionization model solutions for Ne VIII are: $n_H \sim 8 \times 10^{-6}$ cm^{-3}, $N_H \sim 6 \times 10^{19}$ cm^{-2} and line-of-sight thickness is 2.5 Mpc.

Using the KS15 UVB, the results of the photoionization model for the Ne VIII phase of this absorber are shown in Table 2. We obtain the metallicity of the low ionization (and hence high ionization) gas phase to be [X/H] = 0.46. In addition, n_H that is required to reproduce the observed N(Ne VIII)/N(O VI) is a factor of ∼4 higher as compared to what was derived using the HM96 UVB. Also, with the small measured line-of-sight thickness (l = 22 kpc), this absorber too can have a photoionized origin.

4.4 PG 1148+549 (Meiring et al. 2013)

Three Ne VIII absorbers at z_{abs} = 0.68381, 0.70152 and 0.72478, respectively, were observed towards the line of sight of the QSO PG1148+549. Here the authors using the HM96 UVB, concluded that photoionization models cannot explain the Ne VIII absorption due to their measured unrealistically large cloud sizes (>1 Mpc). For z_{abs} = 0.68381, the metallicity reported by Meiring et al.

[5] The photoionization model for the low ions detected in this absorber are discussed in detail by Howk et al. (2009) where the observations were carried out by the *FUSE*. Using HM01 UVB and constraining the ionization parameter using the column density ratios of N(O IV)/(C III), N(O III)/(O IV) and N(O IV)/(O VI), the metallicity reported for the low ionized phase is in the range −0.62 ≤ [X/H] ≤ −0.15.

(2013) is [X/H] = −0.5, while for z_{abs} = 0.70152 and 0.72478, [X/H] > 0.2 and [X/H] > 0.0, respectively, based on photoionization model solutions for the low ions (C III, O III, O IV, N IV) using HM96 UVB. The lower limits in metallicities for the two systems (z_{abs} = 0.70152 and 0.72478) are due to the non-detection of higher H I Lyman series absorption lines.

Using the KS15 UVB and constraining the low ionization gas phase density with the column density ratio of O IV/O III, our photoionization model measured the low ionization (and hence the high ionization) gas phase metallicities to be solar to supersolar. In Table 2, we summarize the photoionization model results of the Ne VIII phase associated with the three absorbers. With the high metallicity measured, as discussed in the previous section, we expect the cooling time-scales to be much shorter in this case if the gas is in collisional equilibrium. Thus it is natural to conclude that Ne VIII is originating from a photoionized gas. The derived line-of-sight thickness (≤20 kpc) also are not unrealistic to rule out the photoionization models.

4.5 PG 1407+265 (Hussain et al. 2015)

Ne VIII absorption is detected in four components (v_{rel} = −150, 75, 0, 60 km s^{-1}) towards the line of sight of QSO PG 1407+265 at z_{abs} = 0.59961. Using the HM05 UVB and solar metallicity, the authors could explain the Ne VIII absorption component at v_{rel}= −150 km s^{-1} under photoionization equilibrium models. Their photoionization model solutions for this Ne VIII absorber are n_H = 5.0 × 10^{-6} cm^{-3}, log N_H = 19.4 cm^{-2} and line-of-sight thickness is l = 186 kpc.

We too, in this work, using the KS15 UVB, also could explain the Ne VIII absorber at v_{rel} = −150 km s^{-1} under photoionization. The photoionization model results for the Ne VIII phase are listed in Table 2. Like the systems discussed above, the metallicity of the low ions (and hence of the high ions) for this absorber are measured to be supersolar. Here the n_H is a factor of ∼3 higher as compared to what have been reported by Hussain et al. (2015) from their photoionization model. With even small line-of-sight thickness (l = 38 kpc) measured with the updated UVB, photoionization too proves to be the natural explanation for this absorber.

4.6 Discussions

The line-of-sight thickness $l \geq$ 100 kpc measured for the two photoionized absorbers: z_{abs} = 0.20701 towards HE 0226−4110 and z_{abs} = 0.32566 towards 3C 263, as discussed above, are still large. However, at low-z, such large cloud sizes are comparable to the sizes of oxygen-rich haloes of isolated star-forming galaxies (see Tumlinson et al. 2011; Werk et al. 2013, 2014) and of the CGM traced by O VI absorbers (see Muzahid 2014).

Given the supersolar metallicities measured in most of the photoionized Ne VIII absorbers, it is interesting to see whether normal galaxies could enrich such Ne VIII bearing gas clouds. Peeples et al. (2014), accounting for the total mass of metals produced by $z \sim 0$ galaxies, estimated that 20–25 per cent of total metal mass produced remains in galaxies i.e. in stars, interstellar gas and interstellar dust. The remaining 75–80 per cent can be distributed in the outskirts of galaxies. Using this fact, we can estimate the stellar mass of galaxies required to enrich Ne VIII bearing clouds. For that, we use the relation between the total mass of metal oxygen produced by galaxies (via a Type II supernovae) and stellar mass of galaxies (see equation 2 of Peeples et al. 2014). Under the approximation that these absorbers have a spherical geometry, the total mass of metal oxygen, M_{oxy}, in the absorbers is $M_{oxy} \simeq 10^5\,M_\odot(\frac{n_H}{cm^{-3}})(\frac{l}{kpc})^3 Z$. Here l, n_H and Z are, respectively, the line-of-sight thickness, total hydrogen density and metallicity of the absorber.

Assuming that these Ne VIII absorbers are probing less than 5 per cent (out of 75 per cent) of metals seen in the outskirts of galaxies, the stellar mass (in terms of oxygen mass) in these galaxies can be written as

$$\log(M_\star/M_\odot) < [\log(M_{oxy}/(0.05 \times 0.75)) + 1.71481]/1.0146.$$

We find the stellar masses to be $<2 \times 10^{10}\,M_\odot$, even for the largest cloud with thickness of 299 kpc. We convert the stellar masses required for each absorber into luminosities using equation (7) of Paranjape et al. (2015), where we use the typical mass-to-light ratio of 0.5384 in SDSS r band [with $(g - r)$ = 0.4] obtained for the blue star-forming galaxies with stellar masses $<10^{10}\,M_\odot$ (see fig. 4, Paranjape et al. 2015). By comparing these luminosities with the observed luminosity function of galaxies as described in Ilbert et al. (2005), we find that all these associated galaxies can be sub-$L_\star$ galaxies. This is consistent with the detection of sub-$L_\star$ to $L_\star$ galaxies associated with some of the absorbers as discussed in Section 3. Thus, the inferred high metallicities and large cloud thicknesses can be accounted for with only ∼5 per cent or less mass fraction of total metals produced by sub-$L_\star$ galaxies. While this back of the envelope calculation provides a sanity check, detailed understanding of the enrichment and spatial distribution of neon in galaxy haloes require more detections of Ne VIII absorbers and associated galaxy identifications.

5 SUMMARY

Using the updated UVB KS15 at low-z, we reanalyse the intervening Ne VIII absorbers to understand the ionization mechanisms of the Ne VIII systems. The important conclusions are summarized as follows:

(1) Using the updated KS15 UVB, Ne VIII and O VI are simultaneously reproduced in a photoionized gas having total hydrogen densities of n_H = 4 × 10^{-5} to 8 × 10^{-6} cm^{-3}. This, in comparison to HM12, is a factor of ∼3 higher. Also, except for a few, all these photoionized absorbers require near solar to supersolar (Z = 1–3$Z_\odot$) metallicities. The line-of-sight thickness measured for these Ne VIII systems with KS15 UVB is l < 100 kpc (except for one absorber with l = 299 kpc) favouring a photoionized origin for all these absorbers. This is unlike, what have been found from previous studies of the Ne VIII absorbers (except Hussain et al. 2015) with HM96, HM01 and HM05 UVB, where photoionization was ruled out purely based on large line-of-sight thickness (>1 Mpc) of the cloud.

(2) We show that the collisionally ionized gas with solar metallicity and having density above critical density can cool within 10^8 yrs. This will make the detectability of the collisionally ionized Ne VIII phase difficult, unless there is a constant heating source present in the system. The cooling issue can be sorted out if the gas phase metallicity is lower. In a couple of cases, BLAs associated with the Ne VIII absorbers have been reported. The inferred N(H I) is consistent with collisional ionization of Ne VIII gas when the gas phase metallicity is less than that of the low ion phase. In such cases, collisions are possible. Therefore, accurate determination or constraints of BLA absorption associated with the Ne VIII phase is important to distinguish between photoionization and CIE models. Mere line-of-sight thickness arguments cannot rule out the photoionized origin of the Ne VIII phase.

(3) Photoionized with the KS15 UVB, Ne VIII absorbers probe $\lesssim$0.5 per cent of the cosmic baryon density as compared to what have been reported for collisionally ionized Ne VIII gas ($\approx$4 per cent). This is because these photoionized absorbers have 10 times less total hydrogen column densities $\log N_{\rm H} = 17.5$–19.0 cm^{-2} as compared to what one obtain from collisional ionization models.

ACKNOWLEDGEMENTS

We thank the anonymous referee for useful comments. TH acknowledges IUCAA for hospitality and support from Startup Research Grant YSS/2014/000338 (PI: N. Gupta) during the period of this work. SM acknowledges support from European Research Council (ERC), Grant Agreement 278594-GasAroundGalaxies.

REFERENCES

Bajtlik S., Duncan R. C., Ostriker J. P., 1988, ApJ, 327, 570
Bordoloi R., Heckman T. M., Norman C. A., 2016, ApJ, preprint (arXiv:1605.07187)
Bridge C. R. et al., 2010, ApJ, 720, 465
Buote D. A., Zappacosta L., Fang T., Humphrey P. J., Gastaldello F., Tagliaferri G., 2009, ApJ, 695, 1351
Burles S., Tytler D., 1998, ApJ, 507, 732
Chen H.-W., Mulchaey J. S., 2009, ApJ, 701, 1219
Cowie L. L., Barger A. J., Trouille L., 2009, ApJ, 692, 1476
Croom S. M. et al., 2009, MNRAS, 399, 1755
Danforth C. W., Shull J. M., 2005, ApJ, 624, 555
Danforth C. W., Shull J. M., 2008, ApJ, 679, 194
Danforth C. W. et al., 2016, ApJ, 817, 111
Davé R. et al., 2001, ApJ, 552, 473
Dove J. B., Shull J. M., 1994, ApJ, 423, 196
Fang T., Marshall H. L., Lee J. C., Davis D. S., Canizares C. R., 2002, ApJ, 572, L127
Fang T., Canizares C. R., Yao Y., 2007, ApJ, 670, 992
Fang T., Buote D. A., Humphrey P. J., Canizares C. R., Zappacosta L., Maiolino R., Tagliaferri G., Gastaldello F., 2010, ApJ, 714, 1715
Fardal M. A., Giroux M. L., Shull J. M., 1998, AJ, 115, 2206
Ferland G. J. et al., 2013, Rev. Mex. Astron. Astrofis., 49, 137
Francis P. J., Hewett P. C., Foltz C. B., Chaffee F. H., Weymann R. J., Morris S. L., 1991, ApJ, 373, 465
Gaikwad P., Khaire V., Choudhury T. R., Srianand R., 2016a, MNRAS, 466, 838
Gaikwad P., Srianand R., Choudhury T. R., Khaire V., 2016b, preprint (arXiv:1610.06572)
Génova-Santos R., Atrio-Barandela F., Kitaura F.-S., Mücket J. P., 2015, ApJ, 806, 113
Gnat O., Sternberg A., 2007, ApJS, 168, 213
Grevesse N., Asplund M., Sauval A. J., Scott P., 2010, Ap&SS, 328, 179
Gurvich A., Burkhart B., Bird S., 2016, preprint (arXiv:1608.03293)
Haardt F., Madau P., 1996, ApJ, 461, 20 (HM96)
Haardt F., Madau P., 2001, in Neumann D. M., Tran J. T. V., eds, Clusters of Galaxies and the High Redshift Universe Observed in X-rays (Available at http://moriond.in2p3.fr) (HM01)
Haardt F., Madau P., 2012, ApJ, 746, 125 (HM12)
Heckman T. M., Sembach K. R., Meurer G. R., Leitherer C., Calzetti D., Martin C. L., 2001, ApJ, 558, 56
Howk J. C., Ribaudo J. S., Lehner N., Prochaska J. X., Chen H.-W., 2009, MNRAS, 396, 1875
Hussain T., Muzahid S., Narayanan A., Srianand R., Wakker B. P., Charlton J. C., Pathak A., 2015, MNRAS, 446, 2444
Ilbert O. et al., 2005, A&A, 439, 863
Inoue A. K., Iwata I., Deharveng J.-M., 2006, MNRAS, 371, L1
Inoue A. K., Shimizu I., Iwata I., Tanaka M., 2014, MNRAS, 442, 1805
Khaire V., Srianand R., 2013, MNRAS, 431, L53
Khaire V., Srianand R., 2015a, MNRAS, 451, L30 (KS15)
Khaire V., Srianand R., 2015b, ApJ, 805, 33
Khaire V., Srianand R., Choudhury T. R., Gaikwad P., 2016, MNRAS, 457, 4051
Kollmeier J. A. et al., 2014, ApJ, 789, L32
Komatsu E. et al., 2011, ApJS, 192, 18
Leitherer C., Ferguson H. C., Heckman T. M., Lowenthal J. D., 1995, ApJ, 454, L19
Meiring J. D., Tripp T. M., Werk J. K., Howk J. C., Jenkins E. B., Prochaska J. X., Lehner N., Sembach K. R., 2013, ApJ, 767, 49
Miralda-Escude J., Ostriker J. P., 1990, ApJ, 350, 1
Mulchaey J. S., Chen H.-W., 2009, ApJ, 698, L46
Muzahid S., 2014, ApJ, 784, 5
Muzahid S., Srianand R., Bergeron J., Petitjean P., 2012, MNRAS, 421, 446
Muzahid S., Kacprzak G. G., Churchill C. W., Charlton J. C., Nielsen N. M., Mathes N. L., Trujillo-Gomez S., 2015, ApJ, 811, 132
Narayanan A., Wakker B. P., Savage B. D., 2009, ApJ, 703, 74
Narayanan A. et al., 2011, ApJ, 730, 15
Narayanan A., Savage B. D., Wakker B. P., 2012, ApJ, 752, 65
Nevalainen J. et al., 2015, A&A, 583, A142
Nicastro F. et al., 2005a, Nature, 433, 495
Nicastro F. et al., 2005b, ApJ, 629, 700
Nicastro F., Mathur S., Elvis M., 2008, Science, 319, 55
Nicastro F. et al., 2013, ApJ, 769, 90
O'Meara J. M., Burles S., Prochaska J. X., Prochter G. E., Bernstein R. A., Burgess K. M., 2006, ApJ, 649, L61
Palanque-Delabrouille N. et al., 2013, A&A, 559, A85
Paranjape A., Kovač K., Hartley W. G., Pahwa I., 2015, MNRAS, 454, 3030
Peeples M. S., Werk J. K., Tumlinson J., Oppenheimer B. D., Prochaska J. X., Katz N., Weinberg D. H., 2014, ApJ, 786, 54
Penton S. V., Stocke J. T., Shull J. M., 2004, ApJS, 152, 29
Persic M., Salucci P., 1992, MNRAS, 258, 14p
Petitjean P., Webb J. K., Rauch M., Carswell R. F., Lanzetta K., 1993, MNRAS, 262, 499
Pettini M., Zych B. J., Murphy M. T., Lewis A., Steidel C. C., 2008, MNRAS, 391, 1499
Rauch M. et al., 1997, ApJ, 489, 7
Ren B., Fang T., Buote D. A., 2014, ApJ, 782, L6
Richter P., Savage B. D., Tripp T. M., Sembach K. R., 2004, ApJS, 153, 165
Rutkowski M. J. et al., 2016, ApJ, 819, 81
Savage B. D., Sembach K. R., 1991, ApJ, 379, 245
Savage B. D., Lehner N., Wakker B. P., Sembach K. R., Tripp T. M., 2005, ApJ, 626, 776
Savage B. D., Narayanan A., Lehner N., Wakker B. P., 2011, ApJ, 731, 14
Savaglio S., Cristiani S., D'Odorico S., Fontana A., Giallongo E., Molaro P., 1997, A&A, 318, 347
Schechter P., 1976, ApJ, 203, 297
Schmidt M., 1967, ApJ, 149, L39
Schure K. M., Kosenko D., Kaastra J. S., Keppens R., Vink J., 2009, A&A, 508, 751
Scott J. E., Kriss G. A., Brotherton M., Green R. F., Hutchings J., Shull J. M., Zheng W., 2004, ApJ, 615, 135
Shapiro P. R., Giroux M. L., Babul A., 1994, ApJ, 427, 25
Shull J. M., Roberts D., Giroux M. L., Penton S. V., Fardal M. A., 1999, AJ, 118, 1450
Shull J. M., Stevans M., Danforth C. W., 2012a, ApJ, 752, 162
Shull J. M., Smith B. D., Danforth C. W., 2012b, ApJ, 759, 23
Shull J. M., Moloney J., Danforth C. W., Tilton E. M., 2015, ApJ, 811, 3
Siana B. et al., 2010, ApJ, 723, 241
Spergel D. N. et al., 2003, ApJS, 148, 175
Srianand R., Khare P., 1996, MNRAS, 280, 767
Stevans M. L., Shull J. M., Danforth C. W., Tilton E. M., 2014, ApJ, 794, 75
Sunyaev R. A., 1969, Astrophys. Lett., 3, 33
Telfer R. C., Zheng W., Kriss G. A., Davidsen A. F., 2002, ApJ, 565, 773
Tepper-García T., Richter P., Schaye J., 2013, MNRAS, 436, 2063
Thom C., Chen H.-W., 2008, ApJS, 179, 37
Tripp T. M., Savage B. D., Jenkins E. B., 2000, ApJ, 534, L1

Tripp T. M., Sembach K. R., Bowen D. V., Savage B. D., Jenkins E. B., Lehner N., Richter P., 2008, ApJS, 177, 39
Tripp T. M. et al., 2011, Science, 334, 952
Tumlinson J. et al., 2011, ApJ, 733, 111
Vanden Berk D. E. et al., 2001, AJ, 122, 549
Viel M., Haehnelt M. G., Bolton J. S., Kim T.-S., Puchwein E., Nasir F., Wakker B. P., 2016, preprint (arXiv:1610.02046)
Vogel S. N., Weymann R., Rauch M., Hamilton T., 1995, ApJ, 441, 162
Wakker B. P., Hernandez A. K., French D. M., Kim T.-S., Oppenheimer B. D., Savage B. D., 2015, ApJ, 814, 40
Werk J. K., Prochaska J. X., Thom C., Tumlinson J., Tripp T. M., O'Meara J. M., Peeples M. S., 2013, ApJS, 204, 17
Werk J. K. et al., 2014, ApJ, 792, 8
Yao Y., Shull J. M., Wang Q. D., Cash W., 2012, ApJ, 746, 166
Zappacosta L., Nicastro F., Maiolino R., Tagliaferri G., Buote D. A., Fang T., Humphrey P. J., Gastaldello F., 2010, ApJ, 717, 74

This paper has been typeset from a TEX/LATEX file prepared by the author.